

UC Irvine

UC Irvine Previously Published Works

Title

Determination of birefringence and absolute optic axis orientation using polarization-sensitive optical coherence tomography with PM fibers

Permalink

<https://escholarship.org/uc/item/8jk861t5>

Journal

Optics Express, 11(24)

ISSN

1094-4087

Authors

Zhang, Jun
Guo, Shuguang
Jung, Woonggyu
[et al.](#)

Publication Date

2003-12-01

DOI

10.1364/OE.11.003262

Peer reviewed

Determination of birefringence and absolute optic axis orientation using polarization-sensitive optical coherence tomography with PM fibers

Jun Zhang, Shuguang Guo, Woonggyu Jung, J. Stuart Nelson, Zhongping Chen

Beckman Laser Institute and the Center for Biomedical Engineering
University of California, Irvine, California 92612
zchen@bli.uci.edu, junzhang@uci.edu

Abstract: A novel polarization-sensitive optical coherence tomography (PS-OCT) system was developed using polarization maintaining (PM) optical fibers and fiber coupler to measure birefringence properties of samples. Polarization distortion due to PM fibers and coupler can be calibrated with different polarization states during two consecutive A-scans. By processing the analytical interference fringe signals derived from two orthogonal polarization detection channels, the system can be used to measure phase retardation and optic axis orientation. Standard wave plates with different orientation and retardation were used as samples to test the system and calibrating method. We have also applied this system to image biological sample such as beef tendon.

©2003 Optical Society of America

OCIS codes: (170.4500) Optical coherence tomography; (260.1440) Birefringence; (230.5440) Polarization-sensitive devices

References and links

1. D. Huang, E. A. Swanson, C. P. Lin, J. S. Schuman, W. G. Stinson, W. Chang, M. R. Hee, T. Flotte, K. Gregory, C. A. Puliafito, J. G. Fujimoto, "Optical coherence tomography," *Science* **254**, 1178-1181 (1991).
2. M. R. Hee, D. Huang, E. A. Swanson, J. G. Fujimoto, "Polarization-sensitive low-coherence reflectometer for birefringence characterization and ranging," *J. Opt. Soc. Am. B* **9**, 903-908 (1992).
3. J. F. de Boer, T. E. Milner, M. J. C. van Gemert, J. S. Nelson, "Two-dimensional birefringence imaging in biological tissue by polarization sensitive optical coherence tomography," *Opt. Lett.* **22**, 934-936 (1997).
4. M. J. Everett, K. Schoenenberger, B. W. Colston Jr., L. B. Da Silva, "Birefringence characterization of biological tissue by use of optical coherence tomography," *Opt. Lett.* **23**, 228-230 (1998).
5. S. Jiao, G. Yao, and L. V. Wang, "Two-dimensional depth-resolved Mueller matrix of biological tissue measured with double-beam polarization-sensitive optical coherence tomography," *Opt. Lett.* **27**, 101-103 (2002).
6. C. E. Saxer, J. F. de Boer, B. H. Park, Y. Zhao, Z. Chen, J. S. Nelson, "High-speed fiber based polarization sensitive optical coherence tomography of in vivo human skin," *Opt. Lett.* **25**, 1355-1357 (2000).
7. B. Cense, T.C.Chen, B.H. Park, M.C.Pierce, and J.F.de Boer, "In vivo depth-resolved birefringence measurements of the human retinal nerve fiber layer by polarization-sensitive optical coherence tomography," *Opt.Lett.* **27**, 1610-1612 (2002)
8. B.H. Park, C. Saxer, S.M. Srinivas, J. S. Nelson, J.F. de Boer, "In vivo burn depth determination by high-speed fiber-based polarization sensitive optical coherence tomography," *J. Biomed.Opt.* **6**, 474-479 (2001).
9. J. E. Roth, J. A. Kozak, S. Yazdanfar, A. M. Rollins, J. A. Izatt, "Simplified method for polarization sensitive optical coherence tomography," *Opt. Lett.* **26**, 1069-1071 (2001).
10. S. Jiao, W. Yu, G. Stoica, and L. V. Wang, "Optical-fiber-based Mueller optical coherence tomography," *Opt. Lett.*, **28**, 1206-1208 (2003)
11. D.P. Davé, T. Akkin, T.E.Milner and H.G. Rylander III, "Phase-sensitive frequency-multiplexed optical low-coherence reflectometry" *Opt. Commu.* **193**, 39-43 (2001).
12. C. Brosseau, *Fundamentals of polarized light: a statistical optics approach* (John Wiley & Sons, Inc., 1998), Chap. 3.

13. Y. Zhao., Z. Chen, C. Saxer, S. Xiang, J. F. de Boer, J. S. Nelson, "Phase-resolved optical coherence tomography and optical Doppler tomography for imaging blood flow in human skin with fast scanning speed and high velocity sensitivity," *Opt. Lett.* **25**, 114-116 (2000).

1. Introduction

Optical coherence tomography (OCT) is a noninvasive, noncontact imaging modality that can provide micrometer-scale cross-sectional images of tissue microstructure [1]. Polarization-sensitive OCT (PS-OCT) can obtain enhanced image contrast and additional physiological information by studying the polarization properties of biological tissues [2-10]. The ability of PS-OCT to measure birefringence image of tissues has a number of potential clinical application including retina imaging [7] and burn depth determination [8]. Previous PS-OCT systems were free spaced interferometers that used bulk optical components to control the polarization states of light in both the reference and sample arms precisely [2-5]. Since fiber based interferometers offer flexible sample arm designs and distinct advantages in system alignment and handling for clinical application, many investigators have studied PS-OCT systems using single mode (SM) fibers [6-8]. However, control of the polarization state of light incident on the sample is difficult because regular SM fibers exhibit undesirable static and dynamic polarization effects due to fiber imperfections and stress perturbation. Due to the random birefringence in SM fibers, accurate orientation of the optic axis in a sample is difficult to determine. Alternatively, a fiber based PS-OCT system was reported which adopted a bulk optics polarization-sensitive apparatus in the sample arm to control the polarization state precisely [9]. However, the inclusion of a bulk optics wave plate in the sample arm is difficult for endoscopic applications. Recently, a PS-OCT system that used a fiber in the sampling arm was demonstrated to measure the Mueller matrices of samples [10]. It adopted a calibration to eliminate the polarization distortion caused by the optical fibers. However, the technique requires a known thin retarder attached to the sample for calibration when the probe moves, which is not convenient in clinical application. Polarization Maintaining (PM) fibers can preserve the amplitude of components along the axis of a fiber, but the phase information is lost due to the large birefringence in PM fibers. In an OCT system [11], a PM fiber pair composed of two equal length segments of PM fiber spliced at 90° to each other was used to ensure the same path lengths through fast and slow axes of the fiber. This method can be extended to PS-OCT systems to maintain phase information for birefringence determination. In this paper, a PS-OCT system using PM fibers is described that can simultaneously obtain phase retardation information and absolute optic axis orientation in the sample by calibrating dynamically the polarization properties of the moving PM fibers in the sample arm. The system is based on a phase-resolved signal processing method whereby the birefringence information is obtained by processing the analytical interference fringe signals derived from two perpendicular polarization detection channels. Our PS-OCT system does not require extra bulk polarization components between the probe and sample for calibration. This is especially important for implementing endoscopic PS-OCT where adding extra calibration components between the probe and sample will be difficult due to space constraints.

2. Stokes vector and Mueller matrix

The polarization state of a light beam can be described by a Stokes vector S as [12]:

$$S = \begin{bmatrix} I \\ Q \\ U \\ V \end{bmatrix} = \begin{bmatrix} a_x^2 + a_y^2 \\ a_x^2 - a_y^2 \\ 2a_x a_y \cos \varphi \\ 2a_x a_y \sin \varphi \end{bmatrix} \quad (1)$$

Where I,Q,U,V are Stokes parameters, a_x and a_y are amplitudes of two orthogonal components of the electric vector and φ represents the phase difference between the two components. The effect of an optical device on the polarization of light can be characterized by a 4×4 Mueller matrix. The matrix acts on the input state S_1 to give the output state S_2 :

$$S_2 = \begin{bmatrix} I_2 \\ Q_2 \\ U_2 \\ V_2 \end{bmatrix} = MS_1 = \begin{bmatrix} M_{00} & M_{01} & M_{02} & M_{03} \\ M_{10} & M_{11} & M_{12} & M_{13} \\ M_{20} & M_{21} & M_{22} & M_{23} \\ M_{30} & M_{31} & M_{32} & M_{33} \end{bmatrix} \begin{bmatrix} I_1 \\ Q_1 \\ U_1 \\ V_1 \end{bmatrix} \quad (2)$$

In the Poincaré sphere representation, a polarization state S can be represented by a point (Q,U,V) . The Poincaré sphere representation provides a convenient method to evaluate changes of Stokes vectors.

3. Experimental setup and calculation

The schematic diagram of the PM fiber based PS-OCT system is shown in Fig. 1. A broadband light source from a 1310 nm superluminescent diode (AFC Technologies) with a FWHM bandwidth of 80 nm was used as the light source. The light is vertically polarized by an in-line polarizer and then split into reference and sample arms by a 2×2 PM coupler (Canadian Instrumentation & Research Ltd.) with two output pigtails matched in length. The slow axis of the PM coupler is vertical so that the linear polarization state is maintained. In the reference arm, an electro-optic phase modulator (JDS Uniphase) was used to generate a stable carrier frequency at 500 kHz for heterodyne detection. The light is polarized in the modulator along the slow axis of the input and output PM fibers oriented at a 45° angle with respect to the horizontal direction. Thus the reference beam undergoes a round trip through the rapid scanning optical delay (RSOD) line which scans at 500 Hz and returns with a linear polarization at 45° . As a result, the two components of the reflected reference beam before the PM coupler are equal both in amplitude and phase. In the sample arm, a polarization modulator (New Focus) with its optic axes at 45° and -45° is used to generate a phase shift of zero and $\pi/4$ varying at 250 Hz. The corresponding Stokes vectors S_1 and S_2 of the vertically linear and elliptical states stay on the QV plane of Poincaré sphere as shown in Fig. 2. Subsequently, the polarization modulator is connected to two identical PM fibers (OZ Optics) with their slow axes crossed orthogonally. The PM fiber pair can preserve the relative phase of light propagating through the fiber since the group delay between the primary axes is compensated for. The primary axes of the PM fiber pair are orientated at 45° and -45° with respect to the horizontal direction so that the fiber pair acts as a linear phase retarder with its axes at 45° and -45° . On Poincaré sphere, the effect of the PM fiber pair is equivalent to a rotation around the U axis by an angle of δ_f . The rotation is clockwise ($\delta_f > 0$) with the fast axis at 45° or counter-clockwise ($\delta_f < 0$) with the slow axis at 45° . As a result, the Stokes vectors of light passing through the fiber pair will keep on a grand circle in the QV plane. After the PM fiber pair, a probe with a collimator and infinity-corrected objective driven by a translation stage is employed. In the detector arm, the interfered beams were split into vertically and horizontally linear polarization channels by a polarization beam splitter. The fringe signals from the two polarization channels are detected by two photo-detectors (Laser Components, Inc.), then high pass filtered, amplified and digitized by a 12-bit analogue to digital conversion board (dual-channel, 5M samples/s per channel, National Instruments). Using Hilbert transformation [13], the two detected signals can be converted into the complex analytical signals which are processed to yield the corresponding Stokes vectors.

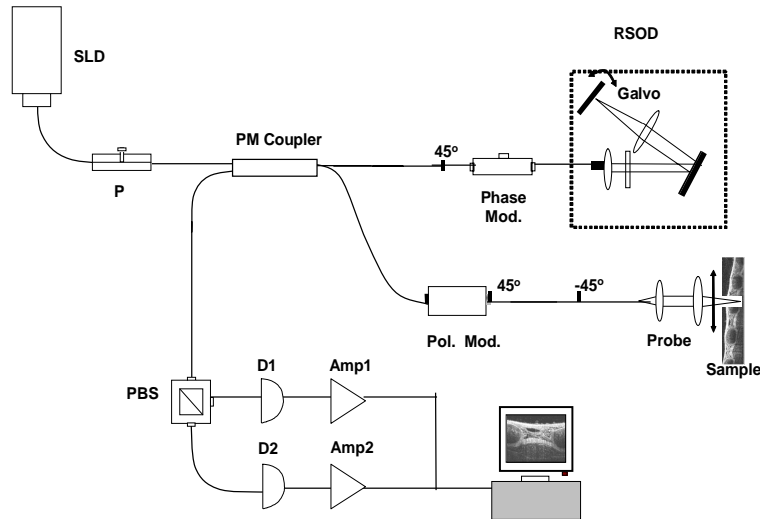


Fig. 1. Schematic of the PM fiber-based PS-OCT system. SLD: superluminescent diode at 1310nm with a FWHM bandwidth of 80 nm. P: Vertically polarized in line polarizer. Pol. Mod.: polarization modulator, Phase Mod.: phase modulator, PBS: polarization beam splitter, RSOD: rapid scanning optical delay line, Galvo: Galvanometer scanner, D1, D2: detectors. Amp1, Amp2: low noise preamplifier.

Due to the minimal mismatch between the lengths of the two output pigtailed of the PM coupler and uncontrolled stress within the coupler, there is an arbitrary phase offset γ in the detected Stokes vectors of the reflected light which should be calibrated dynamically. The sample surface can be used as a reference to calibrate this phase offset. The Stokes vectors S_1 and S_2 of the light reflected from the surface for the two polarization states will remain on the QV plane after round-trip propagation through the PM fiber pairs. The phase offset due to the PM coupler does not alter the amplitudes of the two channels. Therefore, the Stokes vectors S_1 and S_2 of the backward light through the PM coupler will rotate around the Q axis by an angle equal to the phase offset. Because the RSOD scans very fast (500Hz), during two A scans, the phase offset will not change. As a result, the phase offset can be obtained by calculating the angle between the QV plane and the plane determined by S_1 and S_2 . After eliminating the phase offset γ and restoring the Stokes vectors to the QV plane, the phase retardation of the PM fiber pairs δ_f can be easily determined by calculating the rotation angle within the QV plane.

The detected Stokes vector S_o can be obtained as

$$S_o = M_c M_{\text{mod}} M_{pf} M_s M_{pf} M_{\text{mod}} S_i \quad (3)$$

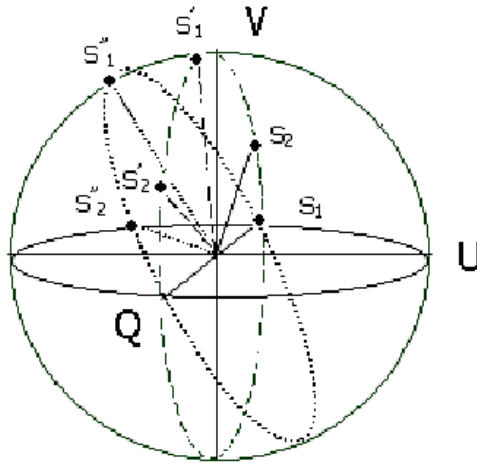


Fig. 2. Poincaré's sphere showing the polarization states of the light. S_1 and S_2 are the Stokes vectors of the light after the polarization modulator in the forward propagation. S'_1 and S'_2 show the possible polarization states of the light reflected from the surface before the polarization modulator in the backward propagation. S''_1 and S''_2 are the possible Stokes vectors of the reflected light from the surface after the PM coupler in the backward propagation.

Where $S_i = [1 \ -1 \ 0 \ 0]^T$ is the Stokes vector of the incident vertically linear polarized light, and the superscript T represents a transpose operation. The Mueller matrix of the PM coupler M_c is given by

$$M_c = \begin{bmatrix} 1 & 0 & 0 & 0 \\ 0 & 1 & 0 & 0 \\ 0 & 0 & \cos \gamma & \sin \gamma \\ 0 & 0 & -\sin \gamma & \cos \gamma \end{bmatrix} \quad (4)$$

With the varying phase shift zero or $\pi/4$, the Mueller matrix M_{mod} of the polarization modulator is

$$M_{\text{mod}} = \begin{bmatrix} 1 & 0 & 0 & 0 \\ 0 & 1 & 0 & 0 \\ 0 & 0 & 1 & 0 \\ 0 & 0 & 0 & 1 \end{bmatrix} \quad \text{or} \quad M_{\text{mod}} = \begin{bmatrix} 1 & 0 & 0 & 0 \\ 0 & \frac{\sqrt{2}}{2} & 0 & -\frac{\sqrt{2}}{2} \\ 0 & \frac{2}{2} & 1 & \frac{0}{2} \\ 0 & \frac{\sqrt{2}}{2} & 0 & \frac{\sqrt{2}}{2} \end{bmatrix} \quad (5)$$

The Mueller matrix of the PM fiber pair M_{pf} can be written as

$$M_{pf} = \begin{bmatrix} 1 & 0 & 0 & 0 \\ 0 & \cos \delta_f & 0 & -\sin \delta_f \\ 0 & 0 & 1 & 0 \\ 0 & \sin \delta_f & 0 & \cos \delta_f \end{bmatrix} \quad (6)$$

The round-trip Mueller matrix of the sample is described by a general linear retarder matrix with the form as

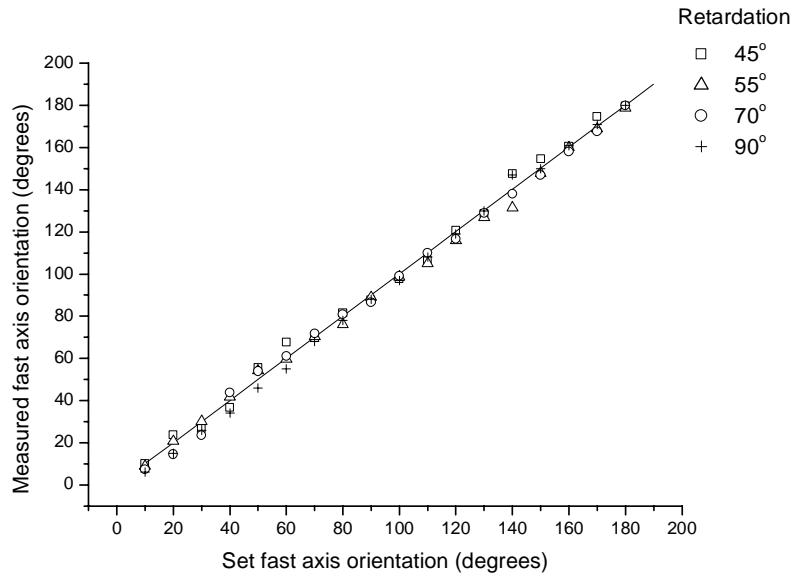
$$M_s = \begin{bmatrix} 1 & 0 & 0 & 0 \\ 0 & 1 - (1 - \cos \delta) \sin^2 2\theta & (1 - \cos \delta) \sin 2\theta \cos 2\theta & -\sin \delta \sin 2\theta \\ 0 & (1 - \cos \delta) \sin 2\theta \cos 2\theta & 1 - (1 - \cos \delta) \cos^2 2\theta & \sin \delta \cos 2\theta \\ 0 & \sin \delta \sin 2\theta & -\sin \delta \cos 2\theta & \cos \delta \end{bmatrix} \quad (7)$$

Where δ is the phase retardation and θ represents the orientation of the fast axis. With the calibration of γ and δ_f , the two components of the Mueller matrix of the sample can be calculated from the Stokes vectors of the incident and detected reflected light with two different M_{mod} from Eq. (3).

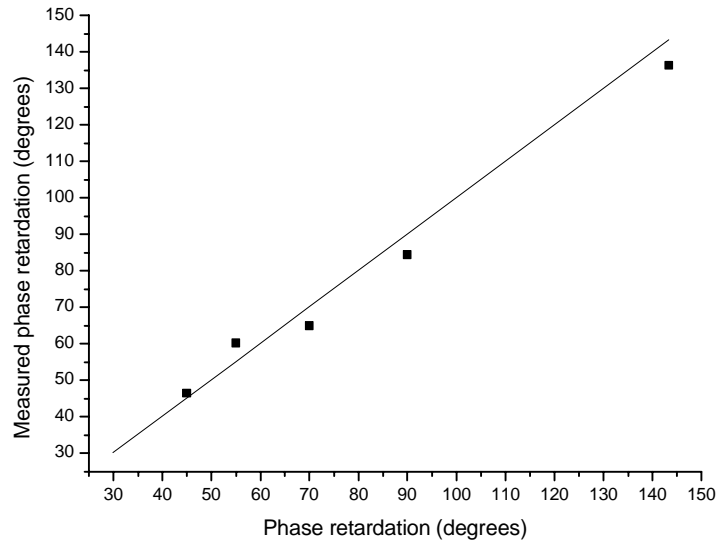
4. Results

To evaluate the system and calibrating method, standard thin wave plates with different retardation (Casix, Inc.) were used as samples. The detected signal reflected from the upper surface was adopted as the reference and the signal reflected from the lower surface was used for calculating the round-trip phase retardation and optic axis orientation. The retardation value and the optic axis orientation of these wave plates were calibrated using a polarimeter (Thorlabs) previously. First, the orientation of the fast axis of the wave plates with different retardations of 45°, 55°, 70° and 90° was measured. In the measurement, the optic axis was varied from 0° to 180° with respect to the horizontal direction in steps of 10° for every wave plate. The measured values of the fast axis orientation versus the set orientation are shown in Fig. 3(a). Second, the values of the phase retardation were measured using wave plates with different retardations of 45°, 55°, 70°, 90° and 143°. The measured retardation of every wave plate for a fixed fast axis orientation of 80° is presented in Fig. 3(b). The experimental data are in good agreement with the expected theoretical values.

To illustrate the performance of the system in biological tissues, beef tendon was imaged. The imaged area is 2 x 1.4 mm. The intensity, phase retardation and fast axis orientation images are shown in Fig. 4. The intensity images are gray coded in logarithmic scale with a range of 50 dB while the phase retardation and optic axis orientation images are gray coded in linear scale from 0° (black) to 180° (white). The birefringent structure shown in retardation and optic axis orientation images is not evident in intensity images. The difference between Fig. 4(b) and Fig. 4(c) implies that additional information may be revealed by optic axis orientation images.

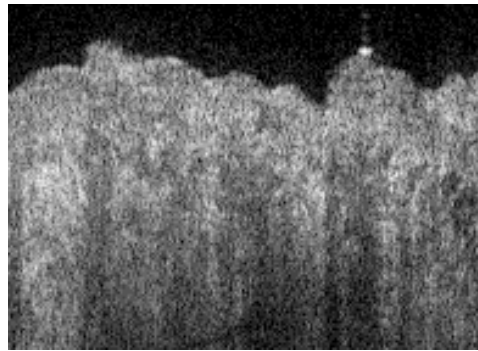



(a)

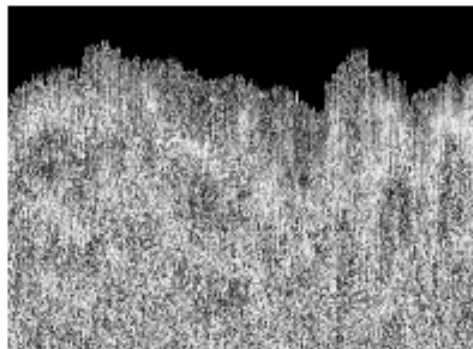



(b)

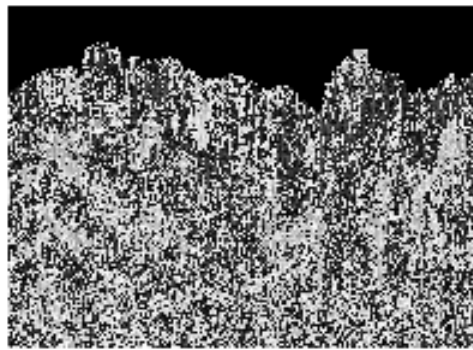
Fig. 3. (a) Measured fast axis orientation as a function of set orientation from 0° to 180° in steps of 10° for different wave plates. The solid line represents the set orientation and the points represent the measured orientation; (b) Measured retardation versus the actual retardation for a fast axis orientation of 80°. The retardation values of the wave plates for measurement are 45°, 55°, 70°, 90° and 143° respectively. The solid line represents the actual retardation and the points represent the measured retardation.



0dB  50dB
(a)



0°  180°
(b)



0°  180°
(c)

Fig. 4. Images of the intensity, phase retardation and optic axis orientation in beef tendon. (a): structural (intensity) image; (b): phase retardation image; (c): fast axis orientation image;

5. Conclusion

We have developed a PM fiber based PS-OCT system. Polarization distortion due to PM coupler and PM fiber pairs was eliminated dynamically using a calibrating method based on the evolution of Stokes vectors in Poincaré sphere. Phase retardation and orientation of the optic axis can be determined simultaneously after calibration. Since there are no additional elements required for calibration, the PS-OCT using a PM fiber can be easily adopted to endoscopic applications.

Acknowledgments

This work was supported by research grants awarded from the National Science Foundation (BES-86924), and National Institutes of Health (EB-00293 and EB-00255, AR-47551, NCI-91717, RR-01192). Institute support from the Air Force Office of Scientific Research (F49620-00-1-0371), and the Beckman Laser Institute Endowment is also gratefully acknowledged.